Polyoxometalate Modified Separator for Performance Enhancement of Magnesium–Sulfur Batteries

Yuanchun Ji, Xinyang Liu-Théato, Yanlei Xiu, Sylvio Indris, Christian Njel, Julia Maibach, Helmut Ehrenberg, Maximilian Fichtner, and Zhirong Zhao-Karger*

The magnesium–sulfur (Mg-S) battery has attracted considerable attention as a candidate of post-lithium battery systems owing to its high volumetric energy density, safety, and cost effectiveness. However, the known shuttle effect of the soluble polysulfides during charge and discharge leads to a rapid capacity fade and hinders the realization of sulfur-based battery technology. Along with the approaches for cathode design and electrolyte formulation, functionalization of separators can be employed to suppress the polysulfide shuttle. In this study, a glass fiber separator coated with decavanadate-based polyoxometalate (POM) clusters/carbon composite is fabricated by electrospinning technique and its impacts on battery performance and suppression of polysulfide shuttling are investigated. Mg–S batteries with such coated separators and non-corrosive $Mg[B(hfip)_4]_2$ electrolyte show significantly enhanced reversible capacity and cycling stability. Functional modification of separator provides a promising approach for improving metal–sulfur batteries.

1. Introduction

The demand of lithium-ion batteries (LIBs) and post-lithium batteries with higher energy density, lower cost, longer lifetime

Dr. Y. Ji, Y. Xiu, Prof. M. Fichtner, Dr. Z. Zhao-Karger
Helmholtz Institute Ulm (HIU) Electrochemical Energy Storage
Helmholtzstrasse 11, Ulm D-89081, Germany
E-mail: zhirong.zhao-karger@kit.edu
Dr. X. Liu-Théato, Dr. S. Indris, Dr. C. Njel,
Dr. J. Maibach, Prof. H. Ehrenberg
Institute for Applied Materials-Energy Storage Systems (IAM-ESS)
Karlsruhe Institute of Technology (KIT)
Hermann-von-Helmholtz-Platz 1, Eggenstein-Leopoldshafen D-76344,
Germany
Dr. C. Njel
Karlsruhe Nano Micro Facility (KNMF)
Karlsruhe Institute of Technology (KIT)
Hermann-von-Helmholtz-Platz 1, Eggenstein-Leopoldshafen
D-76344, Germany
Prof. M. Fichtner
Institute of Nanotechnology (INT)
Karlsruhe Institute of Technology (KIT)
Hermann-von-Helmholtz Platz 1, Eggenstein-Leopoldshafen
D-76344, Germany

for revolutionized technologies from mobile electronics to electric vehicles has triggered tremendous research interest in academies and industries.[1] Because of an abundant reserve of multivalent elements, for example magnesium (Mg), aluminum (Al), and calcium (Ca) and their dendrite-free metal deposition, battery systems based on multivalent metal ions are considered as potential post-lithium energy storage solutions.[2–5] Furthermore, compared with Li metal, multivalent metals have higher volumetric capacities (e.g., 3833 mAh cm^{-3} for Mg vs 2205 mAh cm^{-3} for Li), which plays a crucial role in compact design of portable devices and battery pack for electric cars.[6] However, the realization of high-energy Mg batteries is hampered by lack of high-performance cathode materials. Due to the high charge density of Mg^{2+} (120 C mm^{-3} vs 52 C mm^{-3} for Li^+), the solid-state diffusion kinetics of Mg^{2+} ions in many common intercalation cathodes is sluggish and is often accompanied with irreversible side reactions.[7–9] Alternatively, sulfur as a conversion material may circumvent the sluggish Mg-ion insertion and diffusion process and can be a potential cathode candidate for Mg based system.[10,11] With the perspectives of the high energy density and cost-effectiveness, metal-sulfur batteries are stimulating tremendous research interests.[12,13] Specifically, nonlithium metal-sulfur batteries such as room-temperature sodium-sulfur (Na–S) batteries, potassium sulfur (K–S) batteries and multivalent ion based systems (i.e., Mg–S, Ca–S, and Al–S batteries) are emerging as promising candidates for the next-generation batteries.[14–16]

In contrast to the intensive research and progress of lithium–sulfur (Li–S) battery systems, the research of Mg–S batteries is still in an early stage of R&D. Similar to Li–S batteries, the polysulfide-shuttle is one of the major obstacles hindering the practical viability of Mg–S battery technologies.[10,11] Specifically, sulfur (S_8) in the cathode is first reduced to long-chain polysulfides (S_n^{2-}, $n = 4 – 8$), which easily dissolve in the liquid electrolyte and diffuse to the anode side resulting in severe anode passivation and hence a very fast capacity decay.[17,18] Besides the critical challenges correlated with the sulfur chemistry, it is worth to mention that the suitability of an electrolyte is of crucial importance for the development of practical Mg-S batteries. Some chlorine containing electrolytes synthesized from different chemical combinations such as $Mg(HMDS)_2$–$AlCl_3$

ADVANCED
SCIENCE NEWS
www.advancedsciencenews.com

ADVANCED
FUNCTIONAL
MATERIALS
www.afm-journal.de

(HMDS = hexamethyldisilazide),[19] Mg(TFSI)$_2$–MgCl$_2$ (TFSI = bis(trifluoromethanesulfonyl)imide)[20] have been initially utilized for Mg–S batteries, where sulfur redox mechanism and reversible discharge/charge behavior have been demonstrated. However, these in-situ formed electrolyte systems consist of a complex chemical constitution with various cationic and anionic species including (Mg$_2$Cl$_3$)$^+$ and aluminate ions in chemical equilibria.[21] Moreover, the corrosive nature of chloride ion restricts the practical application of such electrolytes.[22] Recently, the accomplishment in Cl-free Mg-ion conductive salt magnesium tetrakis(hexafluoroisopropyloxy) borate Mg[B(hfip)$_4$]$_2$ (hfip = OC(H)(CF$_3$)$_2$) provide new prospects for Mg–S batteries.[23] Electrochemical and spectroscopic analyses verified the high reversibility of the sulfur redox reactions with the Mg[B(hfip)$_4$]$_2$ electrolyte and also unveiled the detrimental effects of the polysulfide on Mg anode.[24]

During the past decade, different attempts have been made for mitigating the shuttle effect to enhance the reversible discharge capacity and cycling stability of Li–S batteries,[25] including design of appropriate sulfur hosts,[26,27] formulation of new electrolytes and additives,[28,29] as well as protection of anode.[30] Besides, modification of separators has been shown to be an effective approach to suppress polysulfide-shuttling and hence improve battery performance.[31] It has been reported that the functionalized separator can act in various way in improving the performance of Li–S batteries, including physically or chemically anchoring polysulfides;[32–34] electrostatic repulsion of polysulfides;[35–37] as well as increasing the utilization of sulfur species by integrating conductive materials.[31,38,39]

A "polysulfide-phobic" separator prepared by coating 2D VOPO$_4$ sheets onto polypropylene (PP) membrane has been reported.[35] Due to the intramolecular interaction between vanadium and sulfur species, the shuttling of polysulfides can be effectively blocked. The cell incorporated with such an interlayer showed significantly enhanced performance in terms of high reversible capacity and capacity retention.[35] Functional separators based on polyoxometalates (POMs) have also been explored for alleviating polysulfide-shuttling in Li–S batteries.[40] POMs with a general formula [MO$_x$]$_n$ (where M = Mo, W, V and x = 4–7) consist of metal oxide building blocks linked with oxygen atoms, exhibiting well-defined crystal structures.[41] In particular, POMs have interesting redox activities and are capable of multi-electron transfer.[42–53] A silver-POM-based Keggin-type cluster, {Ag^{I}PW$_{11}$O$_{39}$}, has been incorporated into sulfur cathodes to immobilize the polysulfides in Li–S batteries through the interaction of tungsten (W) oxide units with sulfides.[54] Recently, Su et al. have fabricated a functional layer by the direct "slurry-pasting" [PW$_{12}$O$_{40}$]/carbon composite on a polypropylene (PP) separator.[40] Compared with the blank separator, the Li–S battery with the as-prepared POM/Carbon separator exhibited a reversible capacity of around 550 mAh g^{-1} for 120 cycles (an increase of 41%), which was ascribed to the inhibition of the shuttle effect through coulombic repulsion between negatively charged POM and polysulfides.

In this work, we carried out the functionalization of separators with tetrabutylammonium decavanadate (TBA$_3$[H$_3$V$_{10}$O$_{28}$]) clusters (with a typical abbreviation TBA$_3${V$_{10}$}) by electrospinning technique and investigated its application in inhibiting polysulfide shuttle effects for Mg–S batteries. The Mg–S cells were assembled by using Ketjenblack/sulfur (KB/S) composite as cathode, Mg[B(hfip)$_4$]$_2$ in dimethoxyethane (DME) as electrolyte and Mg foil anode. The functional coating consisted of aforementioned POMs and carbon was employed as a polysulfide blocking layer. Additionally, being adherent to the cathode side, the captured sulfur species can be "recycled" via the electrical conductivity of carbon and thus the utilization of sulfur can be enhanced.[55] In particular, the aforementioned POMs coated separators were employed as polysulfide blocking layer; at the same time, the electric conductive carbon coated on one side of the separator can serve as an upper current collect for the cathode and the captured sulfur species can be "recycled" and thus increase the utilization of sulfur.[55] Electrochemical performances of the as-fabricated Mg–S cells have been evaluated. Furthermore, the intramolecular interaction between polysulfide species and decavanadate clusters has been investigated.

2. Results and Discussion

The cathode material was prepared by dispersing elemental sulfur evenly into the conductive carbon matrix Ketjenblack through melt-diffusion at 160 °C and followed by a heat treatment at 300 °C for 1 h to remove the superficial sulfur. The sulfur-loading of the KB/S composites was determined to be ≈50 wt%. (Figure S1, Supporting Information). Mg[B(hfip)$_4$]$_2$/DME electrolyte (0.3 м) was prepared according to literature.[24] The common vacuum filtration has been considered as a straightforward method for separator coating and was initially applied in this study. However, inhomogeneity of the coating and detachment of functional layer from original separator were observed. In fact, electrospinning is a versatile and controllable method to distribute uniform composite fibers directly on the surface of a substrate. It has been utilized to modify the separators for improving mechanical strength and electrolyte wettability.[56] Moreover, electrospinning technique also enables coating functional materials onto conventional separators forming an interlayer to prevent polysulfide shuttle in metal–sulfur batteries.[57] The functionalized separators used in this study were fabricated by electrospinning. Typically, a mixture of TBA$_3${V$_{10}$} based POM, Super P and polyvinylidene fluoride (PVDF) was ground manually at a mass ratio of 1:6:3 for 30 min, then dispersed in N-methyl-2-pyrrolidone (NMP). The slurry mixture was then loaded onto one side of a Whatman C type separator by electrospinning. (Details about the electrospinning procedures can be found in SI). A uniform coating of TBA$_3${V$_{10}$} based POM with a mass loading of 0.5 mg cm^{-2} on the glass fiber separator was obtained. As shown in **Figure 1**, SEM images show the structure of the as-fabricated functional separator with a 10 wt% of POM denoted as es.-POM/C (Detailed preparation can be found in Supporting Information). Compared with pristine glass fiber (Figure 1a), the es.-POM/C separator is uniformly covered with well-defined nanoparticles (Figure 1b,c), which is further confirmed by EDX mapping of elements C, O, and V, the compositions of the POM and Super P carbon (Figure 1d). In addition, Figure S2 in Supporting Information shows the particle size distribution of the POM composites indicating an average size of 50 nm. The thickness of the coating layer on the fibrous and sponge-like separators is estimated to be ≈10 μm.
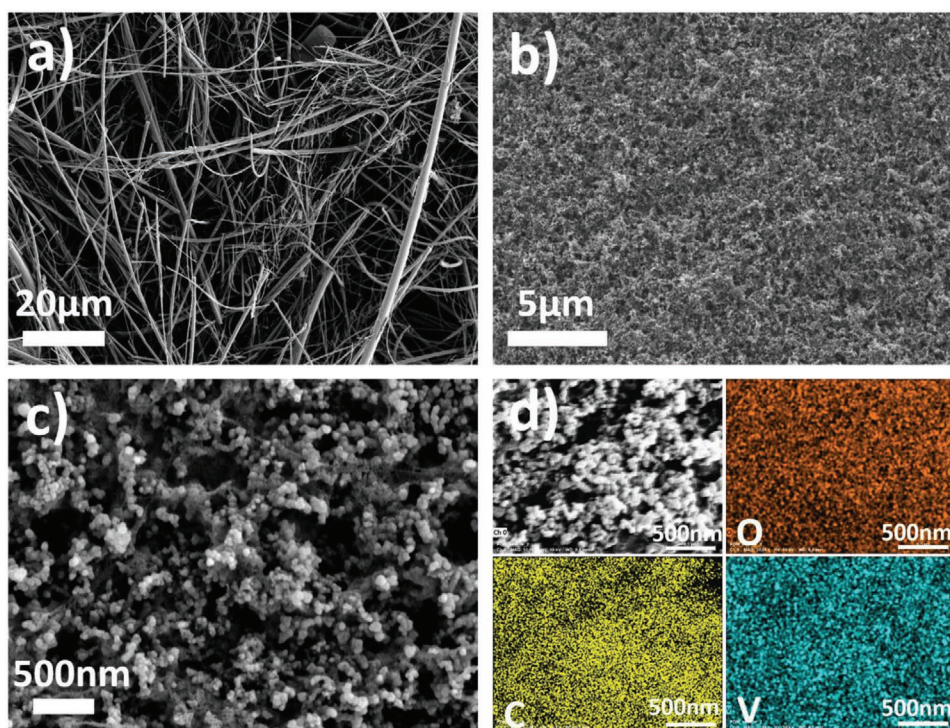
Figure 1. SEM images of a) pristine Whatman glass fibers; b,c) es.-POM/C separator and d) EDX mapping of elements oxygen, carbon, and vanadium of a selected area in es.-POM/C separator.

To visually demonstrate the function of es.-POM/C separator on the suppression of polysulfide diffusion, H-type glass cells were assembled, in which tetraglyme solution of MgS_n (0.04 м, based on Mg^{2+}-ion) was injected in the left chamber and pure tetraglyme solvent on the right side. As shown in Figure S3 in Supporting Information, in the H-type cells in the upper row with the blank separator, the red-brown polysulfides gradually passed through the separator from left to right in 24 h. In contrast, no obvious polysulfide diffusion was observed from the cells in the lower row with es.-POM/C separators after the same duration of time. After 96 h, a slight color change in the right chamber can be seen, which indicated that the es.-POM/C separators can more effectively suppress the polysulfide diffusion than the pristine glass fiber separators.

To examine the function of the es.-POM/C separator for battery cycling stability, different coin cells were assembled with pristine glass fiber separators, carbon coated es.-C and POM coated es.-POM/C separators, respectively. The sulfur loading of the cathode is approximately 1 mg cm^{-2} (The preparation details can be found in Supporting Information). The initial cycles of galvanostatic discharge/charge profiles with pristine separator displayed a relatively flat discharge voltage plateau at about 1.5 V, followed by a sloping region until a cut-off voltage of 0.5 V was reached, indicating a stepwise reaction pathway (**Figure 2**a). Notably, the discharge potential plateau slightly increased after the first cycle, accompanied with an obviously increased coulombic efficiency, which could be ascribed to the formation of fresh and reactive Mg deposits after the first charge process. However, the capacity dropped rapidly after 10th cycle from an initial 460 mAh g^{-1} to a final ≈310 mAh g^{-1} at 0.1C (≈167 mA g^{-1}). In comparison, the Mg–S cells with es.-C

separator demonstrated an improved cycling performance, delivering a discharge capacity of 190 mAh g^{-1} at 30th cycle as shown in Figure 2b. In addition, the discharge-charge profiles exhibit a flat discharge voltage plateau at about 1.5 V followed by a slope. Nevertheless, the voltage gap of ≈0.7 V between the charge and discharge was identified with both types of cells, implying that the carbon coating on the separator could not contribute to reducing the overpotential during charge. Notably, the capacity of the Mg–S cells with es.-POM/C separator increased in the initial 15 cycles (from 360 mAh g^{-1} at 1st cycle to 450 mAh g^{-1}), which might be ascribed to an activation process (Figure 2c,d). The batteries showed a stable cycling performance with a capacity of approximately 400 mAh g^{-1} after 50th cycle and a slight decay to 320 mAh g^{-1} until 100th cycle. The capacity retention was about 89%, which is higher than that of the batteries assembled with es.-C separators (47%). In addition, except for the first cycle, the coulombic efficiency of the battery with es.-POM/C remained around 95% after 50 cycles indicating an efficient polysulfide inhibition and hence a promoted reversibility of the sulfur redox chemistry in the as-designed Mg–S battery prototype during cycling.

Further, we evaluated the rate capability of the Mg-S batteries with es.-POM/C separator at current densities from 0.05–1 C (**Figure 3**). The discharge-charge profiles at the current density of 0.05, 0.1, and 0.2 C present well-defined discharge voltage plateau at around 1.5 V and charge voltage plateau at around 2.0 V, respectively (Figure 3a). While at the current density of 0.5 and 1 C, the discharge–charge profiles indicate no distinct voltage plateau, which might be due to the limited sulfur conversion kinetics in Mg-based systems. Moreover, it was noted that a voltage hysteresis of the Mg–S batteries assembled with
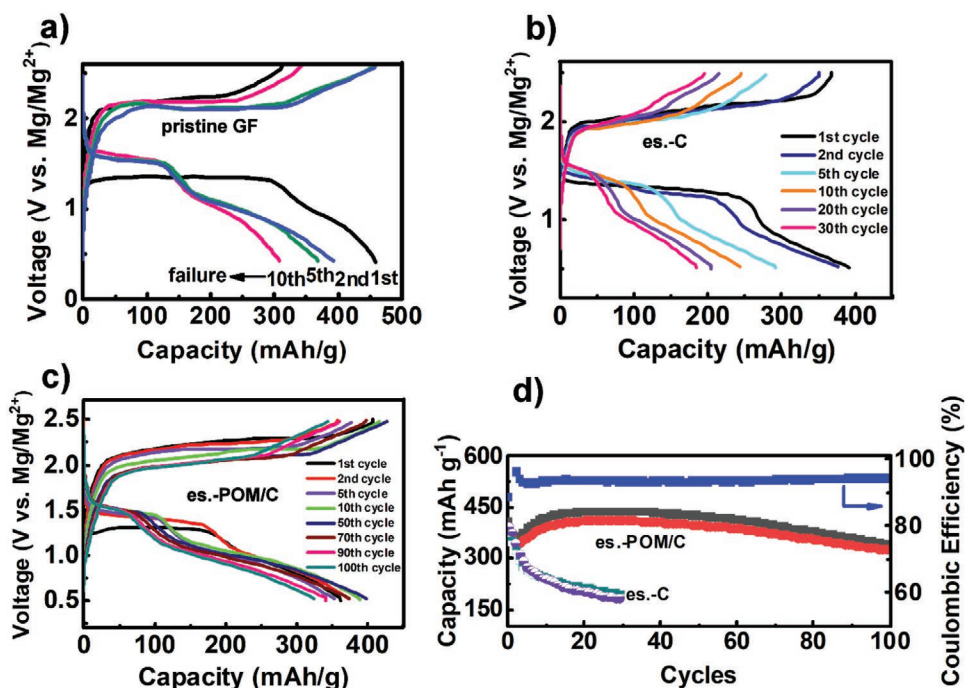
Figure 2. Charge-discharge profiles of Mg–S cells with a) pristine separator; b) electrospun-Super P carbon coated glass fiber separator (abbreviated as es.-C); c) electrospun-POM/C coated glass fiber separator (es.-POM/C); d) Comparison of cycling performance of Mg–S cells equipped with different separators.

es.-POM/C still remained about 0.65 V, which is slightly lower than those of the above mentioned other cells with blank or carbon-coated separators. Nevertheless, it leads to a relatively

low energy efficiency. The battery showed reversible capacities between 650 mAh g^{-1} (at 0.05 C) and 50 mAh g^{-1} (at 1 C) (Figure 3b). To investigate its origin, the CV was measured
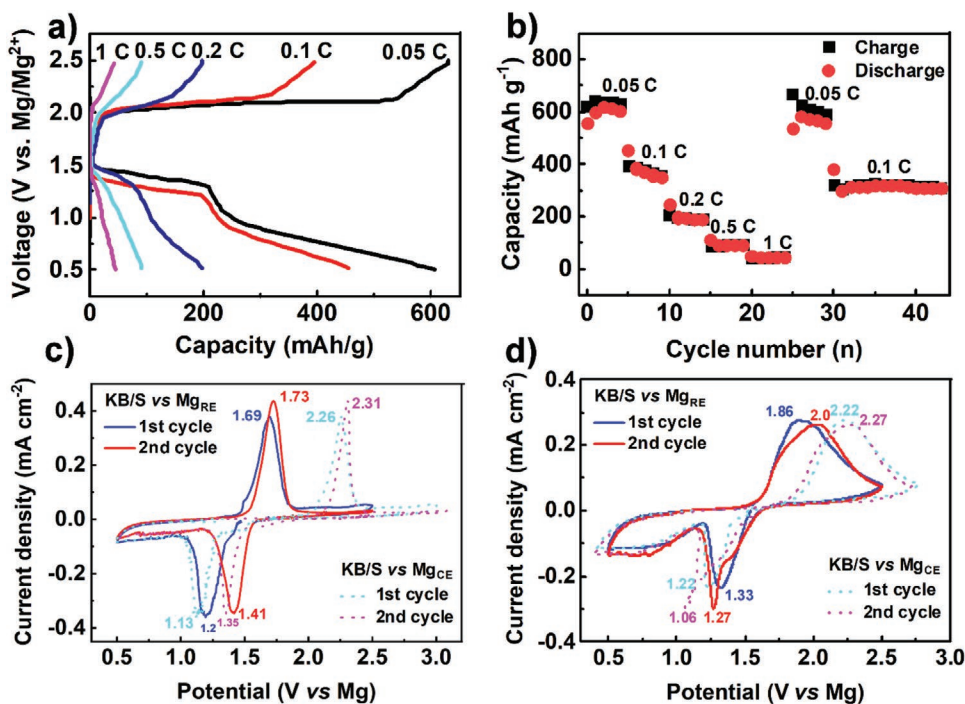

Figure 3. Further electrochemical performance of Mg–S cells with es.-POM/C modified separators: a) voltage profiles and b) rate performance at different C-rates; CVs of Mg–S cells in a three-electrode setup at a scan rate of 0.1 mV s^{-1} c) with pristine glass fiber separator and d) with es.-POM/C modified separator.

**ADVANCED
SCIENCE NEWS**

www.advancedsciencenews.com

**ADVANCED
FUNCTIONAL
MATERIALS**

www.afm-journal.de

with a three-electrode cell (PAT-Cell from EL-CELL) using KB/S as working electrode (WE) and Mg foil as the counter and reference electrodes (Mg_{CE} and Mg_{RE}), respectively. Typical CVs of the cells with pristine glass fiber separator and es.-POM/C for first two cycles are shown in Figure 3c,d. For the cell with pristine glass fiber, during the first anodic scan, the main reduction peak of sulfur appeared at 1.20 V, and the oxidation peak at 1.69 V in the reverse scan. In the subsequent CV cycles, both the cathodic and anodic signals appeared at higher potentials (1.41 and 1.73 V, respectively), which is consistent with the discharge/charge profiles with slightly increased voltages after the first cycle. The small shoulder signals in the CVs indicate a multistep reaction in Mg–S cells. The redox signals at 1.41 and 1.73 V (versus Mg_{RE}) in the second cycle represent a voltage hysteresis of about 0.32 V between the reduction and oxidation of sulfur in the Mg–S system with pristine glass fiber. In the meanwhile, the potentials versus Mg_{CE} were recorded. As shown in Figure 3c, the representative CV curve for the second cycle indicates that the reduction peak for sulfur is located at a slightly lower potential of 1.35 V compared with the peak value versus Mg_{RE}. However, the oxidative signal substantially shifted up to 2.31 V (with a voltage difference of 0.58 V), implying that the recharge of the sulfur cathode was restricted by the half-reaction at the Mg_{CE}. In contrast, the CVs of the cell with es.-POM/C (Figure 3d) indicate that the voltage difference of oxidation peak in the second cycle (versus Mg_{RE} and versus Mg_{CE}, respectively) is about 0.27 V, reflecting a much less polarization of Mg anode. Moreover, the oxidative CV signals for the cell with es.-POM/C became notably broad, which could be correlated with the chemical interaction between vanadate moieties and sulfide species and will be discussed later.

It needs to be mentioned that the influence of the amount of POM in the coating layers on the battery performance has also been checked, that is, separators coated with 5 wt% of POM (es.-5% POM/C) and 20 wt% of POM (es.-20% POM/C) were also fabricated by electrospinning under the same conditions. Figure S4, Supporting Information, presents the charge–discharge profiles and cycling stability of the Mg–S cells with these as-prepared separators, where well-defined voltage plateaus in discharge curves (≈1.5 V) and charge curves (≈2.1 V) are exhibited. However, the performance of the cells with es.-5% POM/C is inferior to those with es.-POM/C (with 10 wt% POM) in terms of severe capacity decay (from 420 mAh g^{-1} in 2nd cycle to 200 mAh g^{-1} after 30 cycles and 100 mAh g^{-1} after 100th cycle) and low coulombic efficiency. In the case of es.-20% POM/C, the cells showed relatively stable cycling stability in the first 20 cycles (Figure S4d, Supporting Information). Interestingly, the batteries could deliver a capacity of around 230 mAh g^{-1} in the 2nd cycle (150 mAh g^{-1} after ten cycles) at the upper discharge plateau (≈1.5 V), which is higher than the corresponding values of the cells with es.-POM/C containing 10 wt% POM. This could be ascribed to the prominent interaction between polysulfide species and the POM, which will be discussed in the following section. However, these cells suffered from overcharging in the initial cycles and rapid capacity fade after 20 cycles. To sum up, the es.-POM/C containing 10 wt% POM showed the best compromise towards enhancing the Mg–S battery performance in terms of reversible capacity, cycling stability, and coulombic efficiency.
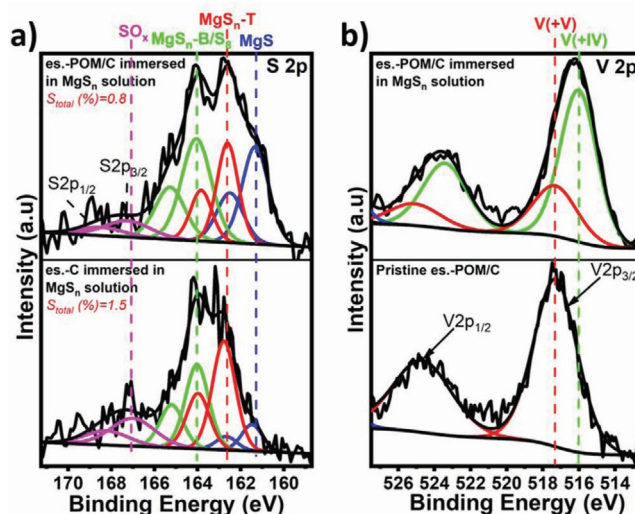

Figure 4. High-resolution XPS analysis. S 2p spectra of a) es.-C (bottom) and es.-POM/C separator immersed in MgS_n solution (upper); V 2p spectra of b) as-fabricated es.-POM/C separator (bottom) and es.-POM/C separator immersed in MgS_n solution (upper). All the samples were measured after drying.

To gain more understanding of the polysulfide inhibiting mechanism of the POM species, X-ray photoelectron spectroscopy (XPS) was implemented in this study. Magnesium polysulfide solution were prepared according to literature,[19] that is, Mg and sulfur powder was ball milled under moderate conditions under argon; the powder mixture was transferred to a glass vial with tetraglyme and stirred for days at room temperature, resulting in a dark red solution with some grey sediment. Subsequently, the suspension was filtrated and the reddish MgS_n solution was used for separator soaking. The ball-milled mixture of Mg and sulfur denoted as MgS_n powder consists of MgS, amorphous polysulfides and small amount of elemental sulfur (The XPS spectra is shown in Figure S5, Supporting Information).[19] All the samples were treated and transferred for measurements under argon atmosphere. The XPS spectra of the blank es.-POM/C, es.-C and es.-POM/C immersed in MgS_n tetraglyme solution are shown in **Figure 4**. Before XPS analysis, the separator samples were washed with tetraglyme in order to remove excess of MgS_n species on the surface of the separator. Note that due to spin–orbit coupling, the S 2p components consist of doublets ($2p_{3/2}$–$2p_{1/2}$) separated by 1.2 eV with a 2/1 intensity ratio. Only the position of the S $2p_{3/2}$ component will be further analyzed. The doublet with S $2p_{3/2}$ component at 167 eV is the signal of sulfides oxidation species (SO_x), which might be caused by the short time air-exposure during sample transfer for the measurements and have often been observed in other studies.[17,24] Two additional S $2p_{3/2}$ components located at around 162.5 eV (red) and 164 eV are assigned to terminal and bridging sulfur atoms from MgS_n polysulfides (2 > n > 8) (denoted as MgS_n-T and MgS_n-B, respectively) and elemental sulfur (S_8), respectively. Another one located at around 161 eV (blue) is attributed to MgS. As MgS is insoluble in ethereal solvents and the separators were treated with a clear MgS_n solution, the MgS on the separators could originated from the transformation of the polysulfides. It is known that different
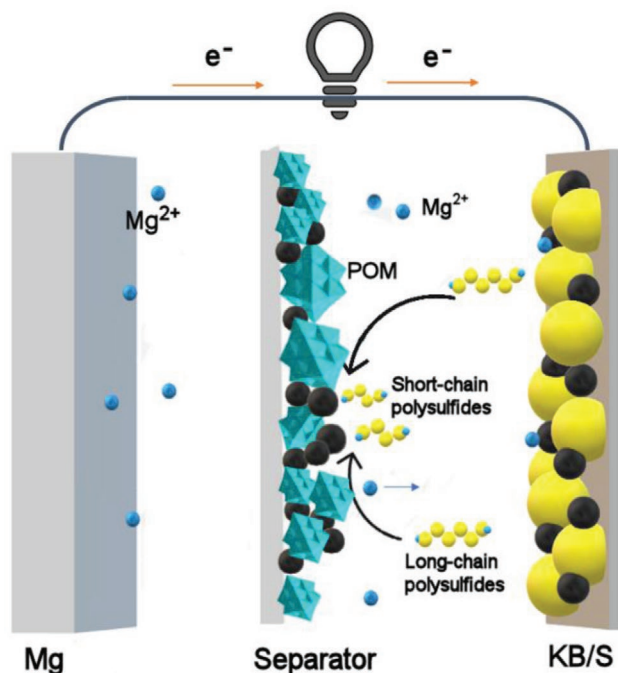
Scheme 1. Schematic illustration of inhibiting shuttle effect by electrospun POMs/carbon separator in Mg–S batteries

polysulfide anions in solution usually co-exist with a series of chemical equilibriums, because the Gibbs free energy of each polysulfide anion is very close.[58] In addition, these soluble polysulfides are thermodynamically instable and can be readily transformed to the stable metal sulfides through proportionate reactions under proper conditions.[59]

Based on Figure 4a, a greater amount of the sulfur species was detected on es.-C separator, which hint a relatively strong adsorption of the sulfur species onto carbon. In fact, carbon materials are well-known adsorbents in the applications of removal of sulfur containing compounds from fuels.[60] In contrast, the S 2p spectra of the es.-POM/C separator indicates a low affinity between sulfur species and POM. Nevertheless, significantly increased amount of MgS implies the promoted conversion of the long-chain MgS_n to the stable sulfide, which could contribute to the enhanced electrochemical performance of the Mg–S batteries with the POM coated separators. In addition, V 2p spectrum of as-fabricated es.-POM/C displayed characteristic V $2p_{3/2}$ and V $2p_{1/2}$ peaks at 517.3 and 524.7 eV respectively, which resemble the V 2p signals of the initial POM material and are assigned to V^{5+} (Figure S6, Supporting Information). However, for the separator soaked in MgS_n solution, a new V 2p doublet appeared at 516.2 and 523.8 eV respectively, which indicate the reduction of V^{5+} to V^{4+}.[61,62] These results suggest that POM clusters can chemically interact with the polysulfide species,[35,63] thus facilitating the transformation of the soluble polysufides to the sulfide. Additionally, with the strong adsorption of the sulfur species on carbon material, the es.-POM/C separator can serve as a shielding layer against the permeation of the polysulfides through the separator moving to the anode side. **Scheme 1** illustrates the proposed the "polysulfide-shielding" mechanism of the separator coating layer comprised of the decavanadate based POM and carbon, where

the sulfur species can be adsorbed onto the carbon material and at the same time the captured sulfide species can be reactivated und reutilized through the synergetic function of the chemical interaction between the long-chain polysulfides and the vanadate moieties and the conductive carbon.

3. Conclusion

In summary, a functionalized separator has been fabricated by coating a composite material consisting of redox active decavanadate-based POM clusters and a conductive carbon. The polysulfide diffusion could be greatly mitigated by employing such functional separators and the Mg–S batteries showed significantly enhanced cycling stability, delivering a reversible discharge capacity of around 320 mAh g^{-1} after 100 cycles with a coulombic efficiency of ≈90%. Moreover, the chemical interaction between vanadate and polysulfides has been verified by XPS, suggesting that the combination of the POM and the conductive carbon attributes to the polysulfide shuttle inhibition and reactivation of the polysulfide species. These results provide a novel approach and guidance for designing innovative functional separators with synergetic effects of polysulfide immobilization and reutilization towards performance enhancement of metal–sulfur battery systems.

Supporting Information

Supporting Information is available from the Wiley Online Library or from the author.

Conflict of Interest

The authors declare no conflict of interest.

Data Availability Statement

Research data are not shared.

**ADVANCED
SCIENCE NEWS**

www.advancedsciencenews.com

**ADVANCED
FUNCTIONAL
MATERIALS**

www.afm-journal.de

[1] P. Bonnick, J. Muldoon, *Adv. Funct. Mater.* **2020**, *30*, 1910510.

[2] Z. Zhang, M. Zhao, M. Xia, R. Qi, M. Liu, J. Nie, Z. L. Wang, X. Lu, *Adv. Funct. Mater.* **2019**, *29*, 1806400.

[3] Z. Li, X. Mu, Z. Zhao-Karger, T. Diemant, R. J. Behm, C. Kübel, M. Fichtner, *Nat. Commun.* **2018**, *9*, 5115.

[4] Z. Li, O. Fuhr, M. Fichtner, Z. Zhao-Karger, *Energy Environ. Sci.* **2019**, *12*, 3496.

[5] Z. Li, B. P. Vinayan, P. Jankowski, C. Njel, A. Roy, T. Vegge, J. Maibach, J. M. G. Lastra, M. Fichtner, Z. Zhao-Karger, *Angew. Chem, Int. Ed.* **2020**, *59*, 11483.

[6] J. Muldoon, C. B. Bucur, T. Gregory, *Chem. Rev.* **2014**, *114*, 11683.

[7] J. Xie, C. Li, Z. Cui, X. Guo, *Adv. Funct. Mater.* **2015**, *25*, 6519.

[8] T. S. Arthur, R. Zhang, C. Ling, P. A. Glans, X. Fan, J. Guo, F. Mizuno, *ACS Appl. Mater. Interfaces* **2014**, *6*, 7004.

[9] P. Bonnick, L. Blanc, S. H. Vajargah, C. W. Lee, X. Sun, M. Balasubramanian, L. F. Nazar, *Chem. Mater.* **2018**, *30*, 4683.

[10] Z. Zhao-Karger, M. Fichtner, *Front. Chem.* **2019**, *6*, 656.

[11] Z. Zhao-Karger, M. Fichtner, *MRS Commun.* **2017**, *7*, 770.

[12] S.-H. Chung, A. Manthiram, *Adv. Mater.* **2019**, *31*, 1901125.

[13] X. Yu, A. Manthiram, *Adv. Funct. Mater.* **2020**, *30*, 2004084.

[14] X. Hong, J. Mei, L. Wen, Y. Tong, A. J. Vasileff, L. Wang, J. Liang, Z. Sun, S. X. Dou, *Adv. Mater.* **2019**, *31*, 1802822.

[15] H. Yang, B. Zhang, Y.-X. Wang, K. Konstantinov, H.-K. Liu, S.-X. Dou, *Adv. Energy Mater.* **2020**, *10*, 2001764.

[16] Y.-X. Wang, B. Zhang, W. Lai, Y. Xu, S.-L. Chou, H.-K. Liu, S.-X. Dou, *Adv. Energy Mater.* **2017**, *7*, 1602829.

[17] T. Gao, X. Ji, S. Hou, X. Fan, X. Li, C. Yang, F. Han, F. Wang, J. Jiang, K. Xu, C. Wang, *Adv. Mater.* **2018**, *30*, 1704313.

[18] T. Gao, S. Hou, K. Huynh, F. Wang, N. Eidson, X. Fan, F. Han, C. Luo, M. Mao, X. Li, C. Wang, *ACS Appl. Mater. Interfaces* **2018**, *10*, 14767.

[19] Z. Zhao-Karger, X. Zhao, D. Wang, T. Diemant, R. J. Behm, M. Fichtner, *Adv. Energy Mater.* **2015**, *5*, 1401155.

[20] T. Gao, S. Hou, F. Wang, Z. Ma, X. Li, K. Xu, C. Wang, *Angew. Chem., Int. Ed.* **2017**, *56*, 13526.

[21] Z. Zhao-Karger, J. E. Mueller, X. Zhao, O. Fuhr, T. Jacob, M. Fichtner, *RSC Adv.* **2014**, *4*, 26924.

[22] C. Wall, Z. Zhao-Karger, M. Fichtner, *ECS Electrochem. Lett.* **2014**, *4*, C8.

[23] Z. Zhao-Karger, M. E. Gil Bardaji, O. Fuhr, M. Fichtner, *J. Mater. Chem. A* **2017**, *5*, 10815.

[24] Z. Zhao-Karger, R. Liu, W. Dai, Z. Li, T. Diemant, B. P. Vinayan, C. Bonatto Minella, X. Yu, A. Manthiram, R. J. Behm, M. Ruben, M. Fichtner, *ACS Energy Lett.* **2018**, *3*, 2005.

[25] A. Rosenman, E. Markevich, G. Salitra, D. Aurbach, A. Garsuch, F. F. Chesneau, *Adv. Energy Mater.* **2015**, *5*, 1500212.

[26] Y. Yuan, G. Tan, J. Wen, J. Lu, L. Ma, C. Liu, X. Zuo, R. Shahbazian-Yassar, T. Wu, K. Amine, *Adv. Funct. Mater.* **2018**, *28*, 1706443.

[27] K. Chen, Z. Sun, R. Fang, Y. Shi, H. M. Cheng, F. Li, *Adv. Funct. Mater.* **2018**, *28*, 1707592.

[28] H. Pan, K. S. Han, M. H. Engelhard, R. Cao, J. Chen, J. G. Zhang, K. T. Mueller, Y. Shao, J. Liu, *Adv. Funct. Mater.* **2018**, *28*, 1707234.

[29] L. Wang, Y. Ye, N. Chen, Y. Huang, L. Li, F. Wu, R. Chen, *Adv. Funct. Mater.* **2018**, *28*, 1800919.

[30] M. Wild, L. O'Neill, T. Zhang, R. Purkayastha, G. Minton, M. Marinescu, G. J. Offer, *Energy Environ. Sci.* **2015**, *8*, 3477.

[31] Y. C. Jeong, J. H. Kim, S. Nam, C. R. Park, S. J. Yang, *Adv. Funct. Mater.* **2018**, *28*, 1707411.

[32] S. Bai, X. Liu, K. Zhu, S. Wu, H. Zhou, *Nat. Energy* **2016**, *1*, 16094.

[33] Y. C. Jeong, J. H. Kim, S. H. Kwon, J. Y. Oh, J. Park, Y. Jung, S. G. Lee, S. J. Yang, C. R. Park, *J. Mater. Chem. A* **2017**, *5*, 23909.

[34] T. Z. Hou, X. Chen, H. J. Peng, J. Q. Huang, B. Q. Li, Q. Zhang, B. Li, *Small* **2016**, *12*, 3283.

[35] Y. He, Y. Qiao, Z. Chang, X. Cao, M. Jia, P. He, H. Zhou, *Angew. Chem., Int. Ed.* **2019**, *58*, 11774.

[36] J. Conder, A. Forner-Cuenca, E. M. Gubler, L. Gubler, P. Novák, S. Trabesinger, *ACS Appl. Mater. Interfaces* **2016**, *8*, 18822.

[37] W. Ahn, S. N. Lim, D. U. Lee, K. B. Kim, Z. Chen, S. H. Yeon, *J. Mater. Chem. A* **2015**, *3*, 9461.

[38] H. Yao, K. Yan, W. Li, G. Zheng, D. Kong, Z. W. Seh, V. K. Narasimhan, Z. Liang, Y. Cui, *Energy Environ. Sci.* **2014**, *7*, 3381.

[39] Y. S. Su, A. Manthiram, *Chem. Commun.* **2012**, *48*, 8817.

[40] W. Yao, L. Liu, X. Wu, C. Qin, H. Xie, Z. Su, *ACS Appl. Mater. Interfaces* **2018**, *10*, 35911.

[41] A. Müller, F. Peters, M. T. T. Pope, D. Gatteschi, *Chem. Rev.* **1998**, *98*, 239.

[42] Y. Ji, J. Hu, J. Biskupek, U. Kaiser, Y. F. Song, C. Streb, *Chem. - Eur. J.* **2017**, *23*, 16637.

[43] Y. Ji, L. Huang, J. Hu, C. Streb, Y. Song, *Energy Environ. Sci.* **2015**, *8*, 776.

[44] J. Hu, Y. Ji, W. Chen, C. Streb, Y. Song, *Energy Environ. Sci.* **2016**, *9*, 1095.

[45] Y. Ji, J. Hu, L. Huang, W. Chen, C. Streb, Y. F. Song, *Chem. - Eur. J.* **2015**, *21*, 6469.

[46] Y. Ji, Y. Ma, R. Liu, Y. Ma, K. Cao, U. Kaiser, A. Varzi, Y. F. Song, S. Passerini, C. Streb, *J. Mater. Chem. A* **2019**, *7*, 13096.

[47] Y. Nishimoto, D. Yokogawa, H. Yoshikawa, K. Awaga, S. Irle, *J. Am. Chem. Soc.* **2014**, *136*, 9042.

[48] H. Wang, S. Hamanaka, Y. Nishimoto, S. Irle, T. Yokoyama, H. Yoshikawa, K. Awaga, *J. Am. Chem. Soc.* **2012**, *134*, 4918.

[49] N. Kawasaki, H. Wang, R. Nakanishi, S. Hamanaka, R. Kitaura, H. Shinohara, T. Yokoyama, H. Yoshikawa, K. Awaga, *Angew. Chem., Int. Ed.* **2011**, *50*, 3471.

[50] D. Ma, L. Liang, W. Chen, H. Liu, Y. F. Song, *Adv. Funct. Mater.* **2013**, *23*, 6100.

[51] J. Hu, H. Diao, W. Luo, Y. F. Song, *Chem. - Eur. J.* **2017**, *23*, 8729.

[52] M. Li, L. Cong, J. Zhao, T. Zheng, R. Tian, J. Sha, Z. Su, X. Wang, *J. Mater. Chem. A* **2017**, *5*, 3371.

[53] H.-Y. Chen, J. Friedl, C.-J. Pan, A. Haider, R. Al-Oweini, Y. L. Cheah, M.-H. Lin, U. Kortz, B.-J. Hwang, M. Srinivasan, U. Stimming, *Phys. Chem. Chem. Phys.* **2017**, *19*, 3358.

[54] J. C. Ye, J. J. Chen, R. M. Yuan, D. R. Deng, M. Sen Zheng, L. Cronin, Q. F. Dong, *J. Am. Chem. Soc.* **2018**, *140*, 3134.

[55] X. Yu, A. Manthiram, *ACS Energy Lett.* **2016**, *1*, 431.

[56] J. W. Jung, C. L. Lee, S. Yu, I. D. Kim, *J. Mater. Chem. A* **2016**, *4*, 703.

[57] M. Liu, N. Deng, J. Ju, L. Fan, L. Wang, Z. Li, H. Zhao, G. Yang, W. Kang, J. Yan, B. Cheng, *Adv. Funct. Mater.* **2019**, *29*, 1905467.

[58] K. Alexey, J. Gun, D. Rizkov, T. Voitsekovski, O. Lev, *Environ. Sci. Technol.* **2007**, *41*, 2395.

[59] D. Zheng, G. Wang, D. Liu, J. Si, T. Ding, D. Qu, X. Yang, D. Qu, *Adv. Mater. Technol.* **2018**, *3*, 1700233.

[60] T. J. Bandosz, in *Activated Carbon Surfaces in Environmental Remediation*, (Ed.: T. J. Bandosz), Vol. *7*, Academic Press, Cambridge, MA, USA **2006**, Ch. 5.

[61] Y. Fan, F. Ma, J. Liang, X. Chen, Z. Miao, S. Duan, L. Wang, T. Wang, J. Han, R. Cao, S. Jiao, Q. Li, *Nanoscale* **2020**, *12*, 584.

[62] U. Zubair, S. Bianco, J. Amici, C. Francia, S. Bodoardo, *J. Power Sources* **2020**, *461*, 228144.

[63] D. Muthuraj, A. Ghosh, A. Kumar, S. Mitra, *ChemElectroChem* **2019**, *6*, 684.